Objective Identification of Cyclones and Their Circulation Intensity, and Climatology

MARK R. SINCLAIR

National Institute of Water and Atmospheric Research, Ltd., Wellington, New Zealand

(Manuscript received 29 May 1996, in final form 31 March 1997)

ABSTRACT

An updated procedure for objective identification and tracking of surface cyclones from gridded analyses is described. Prior smoothing of the raw data with a constant radius spatial filter is used to remove distortions related to the particular grid configuration used and to consistently admit a known scale of disturbance over the domain. Pitfalls of using central pressure or vorticity to infer cyclone intensity are illustrated, and a procedure for obtaining a more realistic areal measure of circulation is described. An automated selection procedure for storms having specific properties is outlined. Case selection is by computer search of a database of cyclone tracks, obtained from an application of the cyclone finding and tracking procedure to an extended series of gridded mean sea level pressure analyses.

A selection of winter season cyclone statistics for both hemispheres is obtained from European Centre for Medium-Range Weather Forecasts analyses. Discrepancies with and between earlier studies appear more related to differing cyclone detection and counting procedures than to any intrinsic variability in analysis quality or cyclone occurrence. Results are found in agreement with the widely accepted manually produced climatologies only when a similar cyclone counting procedure is used. As in previous studies, Northern Hemisphere cyclones form and intensify near the eastern seaboards of Asia and North America, with maximum activity near SST gradients. They move eastward and poleward during their lives before weakening in the Gulf of Alaska and near Iceland. Southern Hemisphere cyclones are more evenly distributed around the hemisphere. They tend to form and intensify in middle latitudes, near SST gradients over open oceans, and near the eastern coasts of South America and Australia, and decay at higher latitudes. There is some evidence that newly formed and intensifying cyclones in both hemispheres possess a tighter inner structure than mature and decaying systems.

1. Introduction

There are many circumstances where it is required to objectively identify cyclones in long series of numerical analyses. Cyclone statistics based on automated finding and tracking of centers have been used to assess or intercompare the performance of numerical models (Akyildiz 1985; Lambert 1988; Le Treut and Kalnay 1990; Murray and Simmonds 1991b; König et al. 1993) or to study the cyclone response to natural or simulated climate variability (Simmonds and Wu 1993; Kidson and Sinclair 1995; Murray and Simmonds 1995). Automated procedures are also now being used to understand the climatological behavior of surface cyclones (Jones and Simmonds 1993; Sinclair 1995, hereafter SI95), anticyclones (Jones and Simmonds 1994; Sinclair 1996), and midtropospheric features (Bell and Bosart 1989; Lefevre and Nielsen-Gammon 1995). In these applications where large sample sizes spanning several years are desirable for meaningful results, labor-intensive manual tracking methods are less feasible. Automated procedures yield consistent, repeatable results and avoid the dependence on subjective decisions whose outcome may vary from day to day and between analysts. As multidecade numerically analyzed datasets become available via the reanalysis efforts at the National Centers for Environmental Prediction (NCEP) and the European Centre for Medium-Range Weather Forecasts (ECMWF), the need for efficient and robust objective feature identification and tracking schemes becomes even more pressing.

Results from objective cyclone identification schemes are highly dependent on the rationale for cyclone selection, as will be illustrated in this study. There is a need to ensure that cyclone detection procedures yield realistic results without introducing bias or missing important disturbances. For example, in the Southern Hemisphere (SH), traditional identification of cyclones as pressure minima overwhelmingly locates most cyclone activity poleward of 60°S (e.g., Le Marshall and Kelly 1981; Lambert 1988). Unfortunately, the evidence from satellite studies (Streten and Troup 1973; Carleton 1979) and general synoptic experience (e.g., Taljaard 1967) is that SH cyclones form and intensify in middle latitudes and decay at higher latitudes. The discrepancy arises because many mobile disturbances in the 40°–60°

Corresponding author address: Dr. Mark R. Sinclair, National Institute of Water and Atmospheric Research Ltd., 301 Evans Bay Parade, Greta Point, P.O. Box 14-901, Kilbirnie, Wellington, New Zealand.
E-mail: m.sinclair@niwa.cri.nz

latitude belt go undetected where the local pressure minimum vanishes because of a superimposed background pressure gradient (Sinclair 1994, hereafter SI94). Thus, results from schemes based on pressure minima are biased in favor of the more intense and/or slower-moving centers south of 60°S. SI94 found that using cyclonic vorticity maxima in place of pressure minima spread the diagnosed zone of cyclone activity throughout a broader range of latitudes between 40° and 65°S, more consistent with satellite imagery and eddy studies (Trenberth 1991).

These ambiguities in cyclone identification are compounded by the scale dependence of point measures of pressure and vorticity. Fine-mesh analyses will resolve many additional weaker disturbances while overly coarse analyses may amalgamate or even obliterate smaller features that are actually important circulation centers. In addition, geographical biases are introduced where resolution varies over the analysis domain, especially when vorticity is used to detect cyclones. Where cyclone behavior from different numerical models is compared, it is crucial to ensure that differences do not merely result from different grid configurations or preprocessing procedures. We can only have confidence in these comparisons when a fixed scale of disturbance is consistently admitted over the domain for all datasets involved.

Finally, there is also a need for an improved measure of the *strength* of a cyclonic circulation. Where cyclone centers have been tracked, cyclone intensity changes are traditionally gauged as mean sea level (MSL) pressure variations following a closed low center. In many case studies, these central pressure falls are compared directly with various cyclogenetic forcings. Unfortunately, this use of central pressure can be misleading. Sometimes, large pressure falls result from rapid migration across a background pressure field rather than from any increase in the strength of the cyclonic circulation (SI95). Sanders and Gyakum (1980) also noted examples where increases in cyclonic circulation were modest, despite huge pressure falls. The alternative use of central vorticity as a measure of cyclone strength reduces this problem (SI95), although it is not difficult to see that systems having similar central vorticity may differ widely in size, structure, and apparent intensity.

This paper describes an updated procedure for the objective identification and tracking of surface cyclones from gridded analyses and estimating their intensity. However, rather than unveiling details of yet another scheme for tracking meteorological features, we illustrate the pitfalls of ignoring the issues raised above and instead propose some revisions to the scheme of SI94 that resolve these questions. Section 2 reviews the components of a robust cyclone finding and tracking procedure, describes a spatial smoothing step that avoids bias resulting from varying grid spacing, and illustrates the adverse consequences of omitting this step. In section 3, we explore the issue of cyclone intensity. We show examples where traditional central pressure fall criteria for diagnosing cyclogenesis are misleading and outline a procedure for obtaining an areal measure of circulation intensity that helps reduce some of these discrepancies.

Automated cyclone finding and tracking schemes are ideally suited to quickly and exhaustively identifying systems possessing certain characteristics from extended series of numerical analyses such as the NCEP or ECMWF reanalyses, or from GCM simulations. This study was initially motivated by attempts to objectively select cases of SH cyclogenesis for a composite study from a 15-yr dataset of ECMWF analyses. Unfortunately, selections from the database of cyclone tracks obtained by SI94 made solely on the basis of central vorticity ranged from tight mesoscale systems to large systems more than 3000 km across, making them unsuitable for compositing. In section 4, we indicate how greater case to case homogeneity can be gained by including additional selection criteria based on circulation. Finally, in section 5, we apply the methodology to a survey of the characteristics of extratropical cyclones in both hemispheres. Results are compared with those from previous studies based on a manual approach.

2. Cyclone identification and tracking

a. Cyclone identification

Any objective scheme for identifying cyclones needs to have a sound physical basis, be robust in application, and yield realistic results. SI94 found that the traditional use of local pressure minima to identify SH cyclones resulted in a bias favoring slow-moving or intense systems south of 60°S because many more mobile centers of cyclonic circulation farther north are not associated with a pressure minimum. By adopting a less restrictive definition of a ''cyclone'' as any center of cyclonic circulation (i.e., not just closed circulations), results were obtained that were in better agreement with satellite and eddy studies, attesting to the improved integrity of the method. Thus, cyclone identification by means of vorticity rather than pressure extrema is seen as a necessary standard to avoid these biases. The reader is referred to SI94 for more discussion of this point.

As well as avoiding bias, use of vorticity captures many additional weaker (but nonetheless, important) secondary rotation centers that would not be detected as pressure minima. These disturbances may comprise preliminary stages of large-scale cyclones and/or be associated with copious precipitation. For example, many of the 30 polar vortices studied by Sinclair and Cong (1992) lacked a pressure mimimum yet were clearly associated with comma-shaped cloud signatures akin to larger frontal cyclones and were readily identifiable as vorticity extrema from ECMWF analyses.

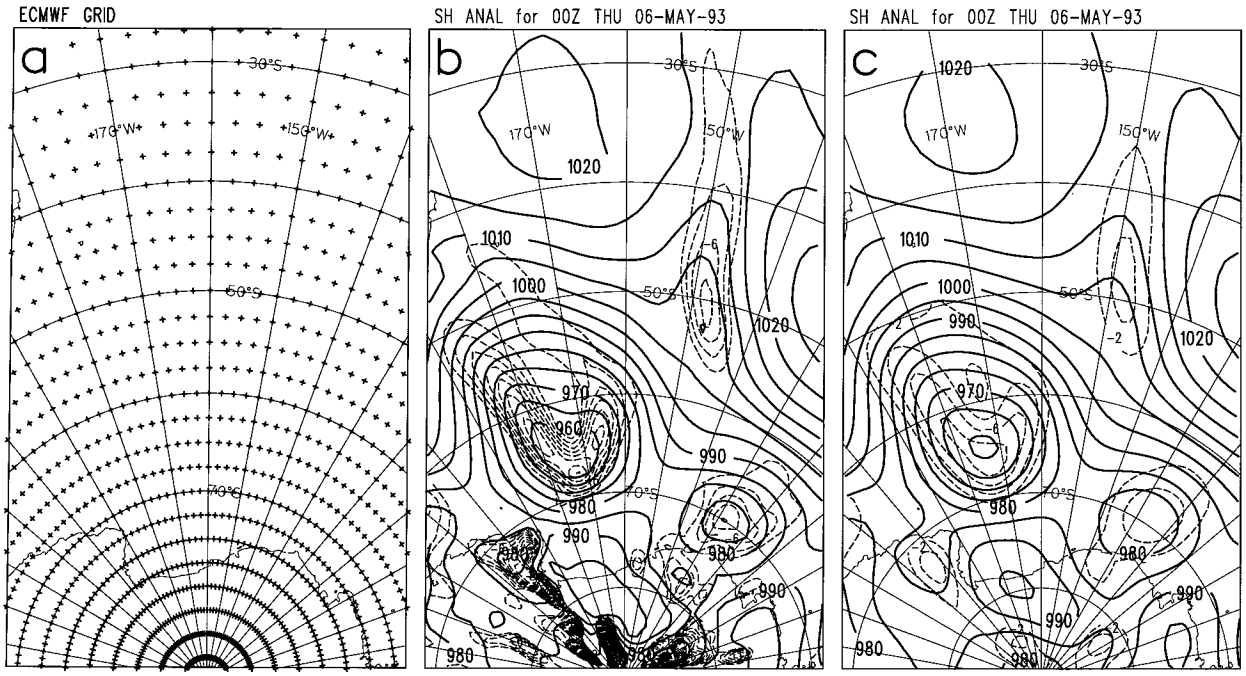

FIG. 1. (a) Section of the ECMWF grid over the high latitudes of the South Pacific Ocean, with grid points shown as crosses. (b) MSL pressure (solid), drawn every 5 hpa and geostrophic vorticity (dashed, every 2 CVU) for 0000 UTC 6 May 1993 as computed without preprocessing. (c) As in (b) except after application of Cressman spatial smoother with r_o of 500 km (one CVU $= -1 \times 10^{-5}$ s^{-1} in the SH and 1×10^{-5} s^{-1} in the NH).

1) SPATIAL SMOOTHING

Because of the scale dependence of vorticity, additional bias can be introduced where grid resolution varies over the domain or between grids. It is crucial to ensure that results are not unwittingly degraded by these effects. There is also a need to control the scale and number of disturbances admitted as cyclones. Fine-mesh analyses may resolve[1] a large number of closely spaced extrema, while overly coarse analyses may merge or even obliterate distinct circulation centers. Spatial smoothing should therefore be used to control the amount of detail included and to ensure the consistent application of a fixed length scale over each grid used.

Analyses of 1000-hPa geopotential from ECMWF on a 2.5° × 2.5° latitude–longitude grid (Fig. 1a) are used to illustrate some of the pitfalls of omitting this crucial step. In Fig. 1b, MSL pressure and geostrophic vorticity are computed from these analyses and contoured directly on this grid. The increased fine detail toward the pole is a result of the decreasing east–west grid spacing. As the vorticity is derived from the Laplacian of the pressure field, it is especially sensitive to the variable grid resolution.

In Fig. 1c, a spatial smoother has been applied before contouring. The smoother follows Cressman (1959). It averages geopotential data at each grid point with all neighboring grid points at a distance $r < r_o$ (here 500 km) using weights of $(r_o^2 - r^2)/(r_o^2 + r^2)$. At a distance of $0.58r_o$ (289 km), this Gaussian-like weighting falls to 0.5. This constant-radius smoothing results in a major reduction in the detail at high latitudes. For example, the unsmoothed analyses in Fig. 1b show the complex cyclone in the Ross Sea near 65°S, 175°W to comprise three closely spaced vortices. However, these merge into a single vortex as a result of smoothing (Fig. 1c). Although these centers possibly represent important features such as frontal waves, localized heating, or secondary centers, most synopticians would regard the low (as analyzed in Fig. 1c) as a single cyclone. Other more distinct vortices are retained as separate features.

Clearly, the choice of an averaging radius is subjective and depends on the context of the study. Smaller values tend to retain large additional weaker vorticity centers not normally thought of as cyclones. Where smaller secondary centers are important to the study in question (say, as initial stages of larger-scale cyclones or precipitation systems), they should be retained by choice of a smaller r_o. However, if the goal of feature identification is to examine ''cyclones,'' it is probably appropriate to smooth with a larger r_o, as in Fig. 1c.

2) LOCATION OF CYCLONIC VORTICITY MAXIMA

Following the application of Cressman smoothing to the geopotential data, cyclones are identified as local

[1] Analysis quality and availability of credible observations will determine the realism of these disturbances.

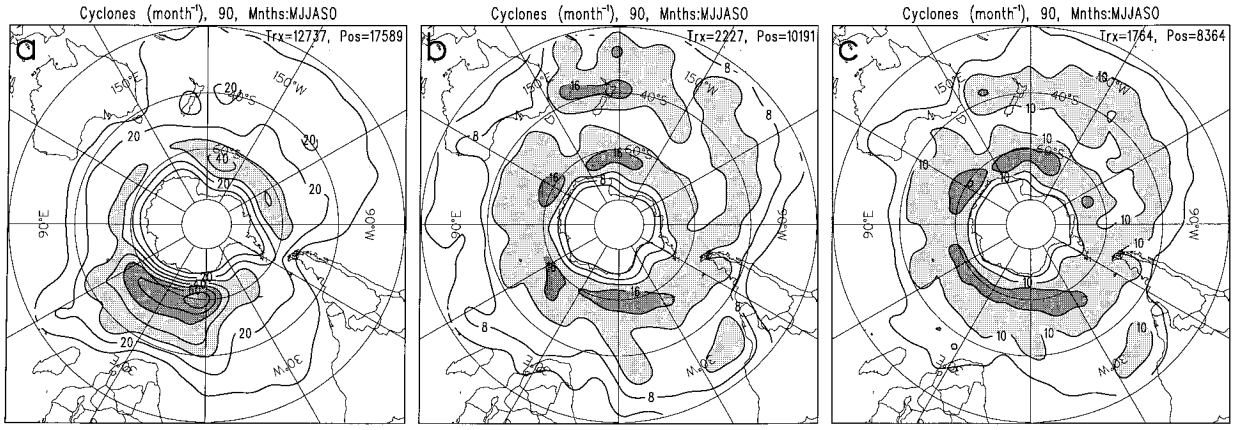

FIG. 2. Counts month^{-1} of vorticity extrema exceeding 1 CVU falling within 555 km (5° lat) of each grid point for the SH during May–October 1990. (a) As computed directly on ECMWF grid with a contour interval of 10, with values exceeding 30 shaded. (b) As obtained following interpolation to a polar stereographic projection, contours every 4, values >10 shaded. (c) As obtained after application of Cressman smoother with r_o of 500 km, every 5, >10 shaded. See text for more details.

maxima of cyclonic gradient wind vorticity (ζ_{gr}) exceeding some threshold. Gradient wind rather than geostrophic vorticity is used because the gradient wind represents a marked improvement over the geostrophic as an approximation to the real wind. Where actual winds at some level above the surface layer are available, these could be used in place of gradient winds. The method of approximating gradient wind used here is described in the appendix. A bicubic spline fit to the ζ_{gr} field was used to identify extrema more accurately between grid points, as described in SI94. Because many of the cyclones located in this way were not associated with a closed circulation (a pressure minimum), the associated pressure was determined by interpolating the pressure field (computed from the 1000-hPa geopotential) to the location of the ζ_{gr} center.

3) SENSITIVITY TO SMOOTHING STRATEGY

Figure 2 illustrates the dramatic consequences for the detection of cyclones when grid configuration and smoothing strategies are varied. The SH is used because of the relative lack of complications from landmasses. Each panel shows the geographical distribution of SH cyclones during May–October 1990 as derived from the same ECMWF data but with differing preprocessing. Cyclones are counted as derived from ECMWF data available twice daily. Vorticity extrema exceeding 1 CVU (-1×10^{-5} s^{-1} in SH, 1×10^{-5} s^{-1} in NH) falling within 555 km (5° latitude) of each gridpoint have been counted, and the results contoured for the same 6-month period. Near land, stationary features such as heat lows and lee troughs have been excluded using a procedure that will be outlined later. In Fig. 2a, cyclones are obtained directly from the ECMWF data on the latitude–longitude grid without preprocessing. In Fig. 2b, data have been interpolated to a polar stereographic projection and smoothed with a 25-point filter (Bleck 1965) before computing vorticity, while in Fig. 2c Cressman smoothing with an r_o of 500 km is used.

It is not surprising that the raw data admits increased numbers of vortices at high latitudes (Fig. 2a) on account of the decreasing grid spacing there. On the other hand, the grid spacing for the polar stereographic domain (Fig. 2b) decreases toward the equator—at 60° latitude it is 1.24 times that at 30°. This results in a small bias favoring cyclone detection at lower latitudes. The constant-radius Cressman smoothing yields a result (Fig. 2c) between these extremes but closer to Fig. 2b. Provided r_o exceeds the largest grid spacing of the data domain, this fixed-radius smoothing removes any latitudinal bias over the grid and consistently admits only spatial variations above a certain fixed length scale. Ensuring this consistency is crucial for meaningful comparisons of cyclone characteristics between different models.

b. Tracking

Tracking of centers enables cyclone motion and intensification rates to be identified and allows consideration of cyclone life cycles, as in SI95. It also enables a database of cyclone tracks to be constructed from which examples can be readily selected for further analysis, such as for case or composite studies, as outlined in section 4 below. Tracking uses an algorithm first developed by Murray and Simmonds (1991a) and modified by SI94. For each center, a prediction of the location, pressure, and vorticity at the next track position is made from past motion, pressure, and vorticity tendency. To start a track, these predictions are based on climatology. Next, a match is attempted between each of these predictions and the set of nearby centers found at the next analysis time (12 h later for ECMWF). The ensemble of successful matches chosen is the one that minimizes a

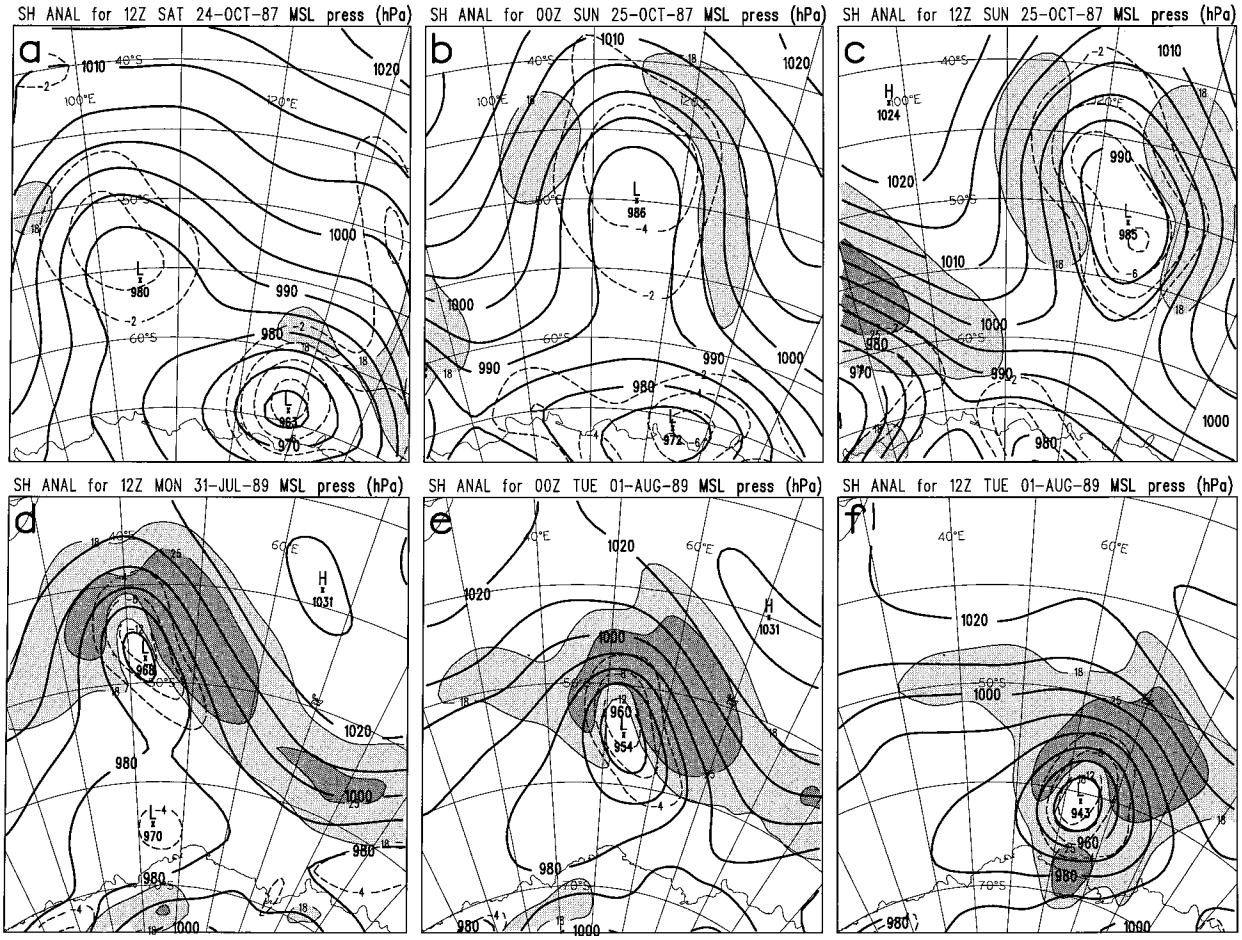

FIG. 3. MSL pressure (solid) and cyclonic ζ_{gr} (dashed) for the indicated times. Areas of gradient wind exceeding 18 and 25 m s^{-1} are shaded. (a)–(c) MSL pressure is drawn every 5 hPa, vorticity every 1 CVU; (d)–(f) these are 10 hPa and 4 CVU.

weighted sum of absolute departures of position, pressure, and vorticity from the predicted values. For more details, see Murray and Simmonds (1991a) and SI94.

c. Elimination of orographic features

Near land, many quasi-stationary orographic features are detected. These arise from features such as heat lows and lee troughs, and from uncertainty in extrapolating to 1000 hPa over high terrain. The tracking revealed that these remained anchored to landmasses. They were eliminated by requiring cyclones spending their entire life over or within 500 km of land to have a total translation of at least 1200 km. This mobility requirement had little effect on systems migrating to or from adjacent seas.

3. Estimation of cyclone strength

Once a cyclone has been identified and tracked, the resulting series of central MSL pressure or vorticity estimates are generally used to gauge cyclone intensity. Unfortunately, these point measures often fail to represent the true strength of a cyclonic circulation or its variation with time, as we now illustrate.

a. Failure of traditional methods

Figure 3 features two situations where central pressure tendency misrepresents cyclone intensity change. Although cyclogenesis is commonly associated with falling central pressure, this is not always the case. Figures 3a–c shows a cyclone south of Australia whose central pressure initially rose about 5 hPa in 12 h as it migrated equatorward about a larger parent low to the south. Despite the rising pressure, the area of cyclonic vorticity and gradient flow about it strengthened and expanded. These circulation increases continued as the low turned southeastward (Fig. 3c).

Conversely, rapidly falling pressure does not always indicate cyclogenesis. The area and strength of the cyclonic circulation in Figs. 3d–f remained more or less constant during a period of central pressure falls ex-

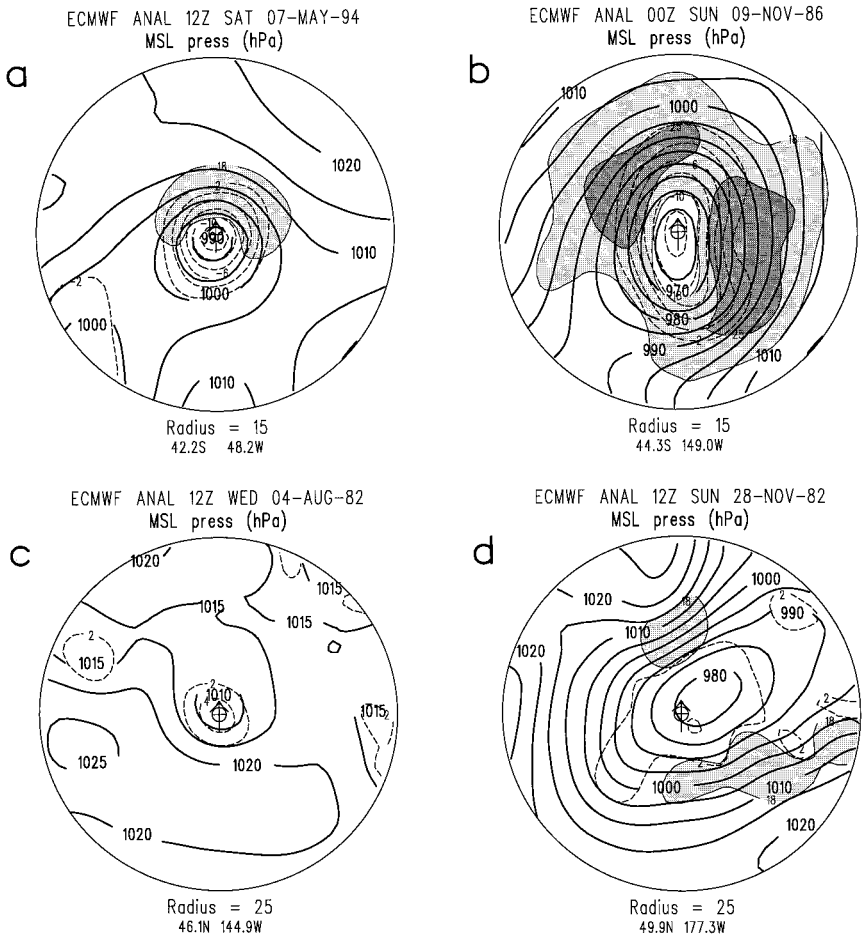

FIG. 4. MSL pressure, ζ_{gr} (every 2 CVU), and gradient wind, as for Figs. 3c and 3d except on a polar grid of radius (a),(b) 15° latitude (1666 km) and (c),(d) 25° (2778 km), at the times and locations indicated with each plot.

ceeding 1 Bergeron[2] (B). In this case, the rapid pressure falls occurred as the circulation system moved quickly toward a region of lower background pressure. Based on mean conditions for August as averaged from 15 yr of twice-daily ECMWF data (not shown), the climatological MSL pressure difference along its path (between Figs. 3d and 3f) is 25 hPa, which is exactly the 24-h pressure fall between these two times.

The use of central vorticity as a measure of cyclone strength is also problematic. Figures 4a and 4b show two cyclones having similar central vorticity of around 11–12 CVU. However, the system in Fig. 4b involving a larger circulation and winds >25 m s^{-1} is clearly the more intense. Furthermore, a transformation from a system like Fig. 4a to Fig. 4b would be regarded as a major cyclogenesis event, despite the absence of any central vorticity change. Examples from the Northern Hemisphere (NH) involving weaker central vorticity are shown in Figs. 4c and 4d. The first (Fig. 4c) was a weak disturbance <1500 km in diameter, while the other (Fig. 4d) was a major circulation system >4000 km across, despite a central vorticity of only ~ 3 CVU. Again, based solely on central vorticity, these two systems would be gauged as being of similar strength!

b. Calculation of cyclone circulation

Circulation, equivalent to the area enclosed by a curve times the mean vorticity over the area (or the line integral of velocity around the boundary of the area), is a more realistic measure of cyclone strength because it takes into account both the size and rotation rate of the system. The main difficulty with circulation calculations lies in defining the region of cyclonic airflow associated with each vortex. This possibly explains why such calculations are seldom made. The outer boundary of a cyclone could be defined by the zero (or some other) contour of vorticity. While this definition is workable

[2] 1 Bergeron = (24 hPa day^{-1}) $\times$ (sinϕ/sin60°), where ϕ is the latitude of the cyclone center (Sanders and Gyakum 1980).

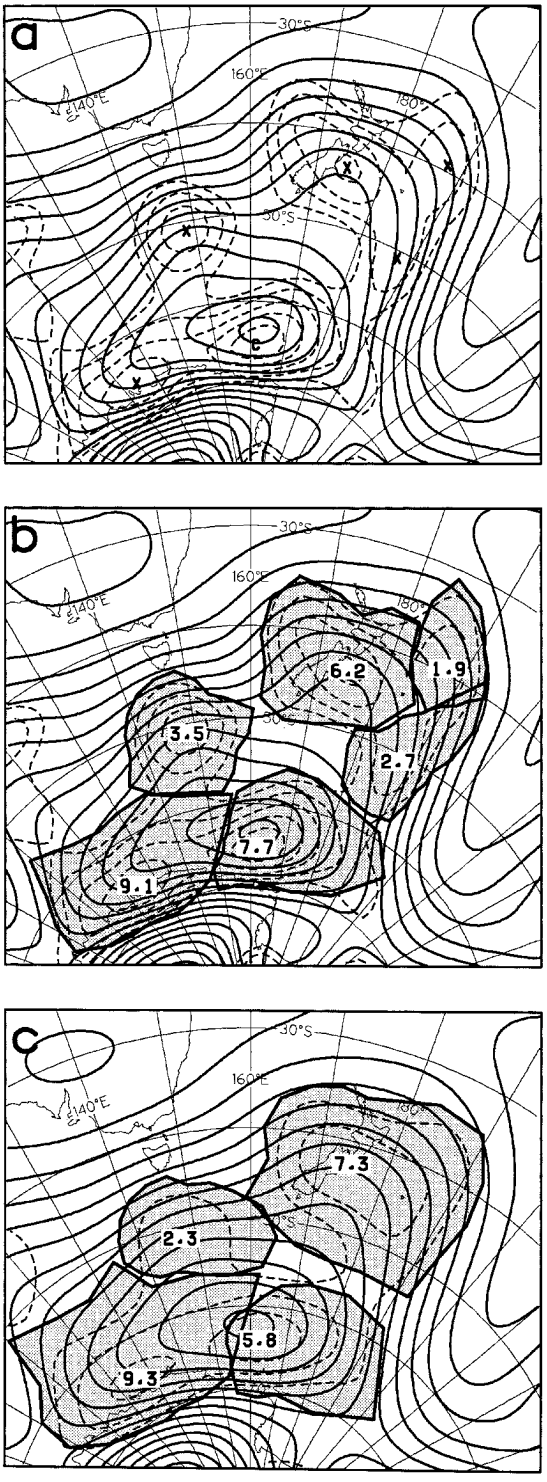

FIG. 5. (a) MSL pressure (solid, every 5 hPa) and cyclonic geostrophic vorticity (dashed, every 1 CVU) for 0000 UTC 1 August 1984. Cyclonic vorticity maxima have been marked ''C'' (closed center associated with a pressure minimum) or ''X'' (open center). Contour labels have been omitted for clarity. (b) As in (a) but with domains for each circulation system outlined and shaded, and circulation values in CU included for each region, for r_o = 500 km. (c) As for (b) except r_o = 1000 km.

for discrete, well-separated vortices, it is common for several centers of rotation to exist within a broad region of cyclonic rotation. Such a situation is illustrated in Fig. 5a. Here, ''closed'' centers are marked with a ''C'' where the vorticity center occurs within 300 km of a local pressure minimum. All other (open) centers are marked with an ''X.'' In all, the complex low pressure system in Fig. 5a contains six rotation centers. Our task is to allocate a domain to each.

The procedure assumes that the region belonging to each vortex just covers the region of decreasing cyclonic vorticity surrounding each maximum. Starting from the location of the cyclonic vorticity maximum, a search is made radially outward for the location where either the vorticity becomes zero or the radial vorticity *gradient* changes sign, whichever occurs first (i.e., is closest to the center). Interpolation is based on a continuous bicubic spline fit to the vorticity field. This procedure is repeated every few degrees of azimuth around a complete circle and, the locations of the boundary points so found, saved. For this procedure, a radial grid spacing Δr of 111 km (equivalent to 1° latitude) and an azimuthal increment $\Delta\theta$ of 0.34906 radians (20°) were used. An overly coarse polar grid tended to produce erratic boundaries, while a finer grid resulted in an unacceptable increase in processing time. To avoid very narrow elongations such as might occur along fronts, boundary points were only permitted to change radius by r/3 km $(20°)^{-1}$ azimuth, while to avoid overlapping domains, vertices that fell inside an adjacent domain were relocated radially inward to the first point outside the neighboring domain.

The cyclone domains obtained by this method are shown in Fig. 5b. Here, an r_o of 500 km has been used for the spatial smoothing. Because of the finite grid increments, there is some slight overlap between some adjacent boundary line segments (but not vertices). Circulation was computed for each cyclone by summing the product $|\zeta_{gr}|r\Delta r\Delta\theta$ over each (r, θ) point in the shaded domain, where r is the radial distance from the cyclone center and Δr and $\Delta\theta$ are the radial and azimuthal increments, respectively. The circulation values obtained for each region are plotted in units of 10^7 m^2 s^{-1}, or circulation units (CU). A circulation of 10 CU is roughly equivalent to a tangential wind component of 10 m s^{-1} at a radius of 1600 km or a mean vorticity of around 1.25 CVU over the same circular area.

The effect of increasing r_o is shown in Fig. 5c. Here, an r_o of 1000 km has been used. This results in merging of the three vortices near New Zealand into a single circulation of strength 7.3 CU. The other three vortices remained intact. Because it involves spatial averaging, circulation is less dependent on effective resolution than point measures. Despite the doubling of the smoothing radius, the circulation for the three vortices south of New Zealand decreased by an average of less than 20% while their central (point) vorticities fell by an average of 40%.

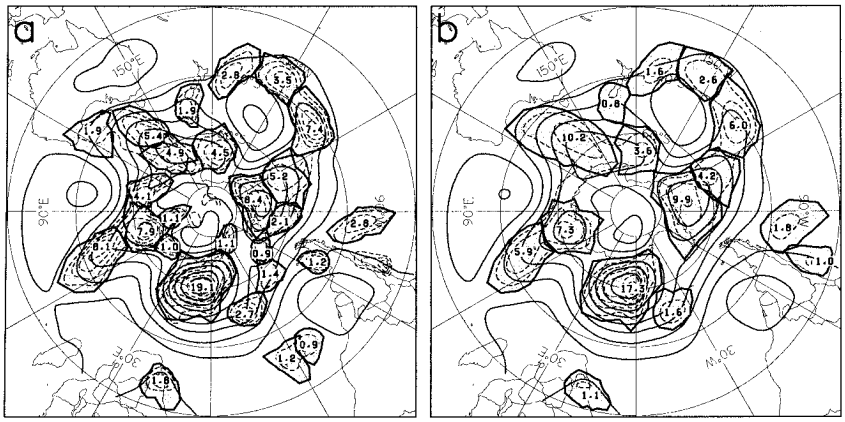

FIG. 6. MSL pressure (solid, every 10 hPa) and cyclonic ζ_{gr} (dashed, every 2 CVU) for 1200 UTC 7 July 1989, with circulation domains and values added, as in Fig. 5, for (a) r_o = 500 km and (b) r_o = 1000 km.

In Fig. 6, vortex domains with associated circulation estimates are shown for the entire hemisphere for 1200 UTC 7 July 1989. A particularly intense 932-hPa low south of Africa has a circulation of 19.1 CU for r_o of 500 km (Fig. 6a) and 17.3 CU for r_o = 1000 km (Fig. 6b). Other less intense systems have smaller circulation values. Three circulations in Fig. 6a of strength 8.4, 2.1, and 0.9 CU in the southeast Pacific merge into a single 9.9-CU vortex centered near 70°S, 100°W at coarser resolution (Fig. 6b). This indicates that some ambiguity remains about what actually constitutes a cyclone. At finer resolution, a single large circulation system may break up into several circulation. In addition, temporal discontinuities may arise where a new secondary development divides a cyclone into two circulations.

c. Circulation estimates for Figs. 3 and 4

Circulation estimates obtained as described above were found to better represent the circulation strength for the situations depicted in Figs. 3 and 4. For the situation in Figs. 3a–c, circulation increased from 5.3 CU through 7.6 CU (Fig. 3b) to 9.3 CU (Fig. 3c), despite the rising central pressure. Conversely, the circulation for the storm in Figs. 3d–f remained remarkably constant (between 12.5 and 12.8 CU) in spite of the 25-hPa fall in central pressure. Likewise, the pairs of cyclones in Fig. 4 having similar central vorticity had widely differing circulation: 5.7 and 13.7 CU, respectively, for Figs. 4a and 4b, and 3.7 and 14.3 CU for Figs. 4c and 4d. Thus, for the cases illustrated, the disparities associated with point measures of pressure and vorticity have been avoided by use of circulation.

In conclusion, circulation estimates show promise in avoiding the discrepancies associated with using central pressure or vorticity to estimate cyclone strength. However, caution must be exercised in interpreting circulation changes following a system within which new secondary centers form.

4. Case selection from a cyclone database

The availability of a database of cyclone tracks can greatly simplify the selection of past storms for case or climatological studies. For example, cyclones having certain intensity characteristics in common are needed for composite studies (e.g., Sanders 1986; Manobianco 1989; Gyakum et al. 1992; Bullock and Gyakum 1993). Automated techniques can expedite the case selection process by avoiding laborious manual examination of thousands of synoptic charts while yielding consistent, repeatable results.

In this section, we outline an automated case selection rationale for exhaustively selecting cyclones possessing specified intensity and geographical characteristics. Our task may be to list all particularly intense winter cyclones (say, those whose circulation attained at least 20 CU or whose central pressure fell below 960 hPa) for the western North Atlantic (say, bounded by 90°–30°E, and 30°–60°N) during November–April for the years 1950–95. Alternatively, we may want a listing of rapidly intensifying cyclones (e.g., those which deepen faster than 1 B or whose circulation increases faster than 6 CU day^{-1}) for the same region.

Case selection is made from a database of cyclone tracks, obtained via the methodology described in this paper. For each cyclone as tracked, the date, latitude, longitude, pressure, vorticity, and circulation are archived for each track point. Selections are made from the database by computer by searching for track points having the desired properties. A cyclone database interface program called TRAX is used to provide a variety of filters for cyclone properties. Cyclones can be selected on the basis of any combination of pressure, vorticity, circulation, movement, geographical location, position in track (start, end, or *n*th), track length (time or distance), and time characteristics. Output can be in the form of contour maps of accumulated statistics as in Fig. 2, or as histograms of cyclone properties (as in SI95), or as text listings

of cyclones having the desired properties. Cyclone tracks and central pressure or vorticity traces can also be plotted.

Although the TRAX software is interfaced to site-specific graphics packages, the heart of the software is the simple logic for cyclone selection. Time filters are applied first. Cyclones can be selected on the basis of year(s) and/or month(s). Other time filters can be added as neccessary. For example, one could select just those periods where the Southern Oscillation index (SOI) is between specified bounds by interfacing with a database of monthly SOI values. In the study of Kidson and Sinclair (1995), composites of cyclone statistics were accumulated for episodes of persistent regional geopotential height anomalies. Geographic filters can be applied to select cyclones within latitude–longitude bounds or those passing within a specified distance from a specified point. This last feature can be used to construct time series of cyclone activity for specific locations. Cyclone translation velocity, computed from the track coordinates, can be used to select cyclones moving in a particular direction and/or faster than a certain speed.

Selection criteria for composite studies need to be carefully chosen to ensure a reasonable degree of case to case homogeneity. We have already seen how cases having similar central vorticity can possess rather different structure (Fig. 4). Figure 7 shows examples of intense cyclones near New Zealand, objectively selected using three different measures of cyclone intensity: central vorticity exceeding 12 CVU (panels a–d), circulation exceeding 14 CU (panels e–h), and both vorticity >10 CVU and circulation >10 CU (panels i–l). These selections were made exhaustively for a region bounded by 30°–50°S and 150°E–150°W from ECMWF data spanning 1980–94. In this instance, the TRAX software generated a list file containing the track coordinates, times, and other properties of all cyclones having the desired characteristics. This file was then read by a plotting program to produce Fig. 7.

Included in Fig. 7 are gradient wind isotachs and contours of gradient wind streamfunction, ψ, obtained by solving $\nabla^2\psi = \zeta_{gr}$ for ψ by successive overrelaxation. This allows easier comparison for cyclones at different latitudes, since, unlike pressure or geopotential, the ψ field corresponding to a given wind field is latitude independent. Contours of ψ are scaled by $2\Omega \sin(-60°)/(10\ g)(-1.2874 \times 10^{-6})$ to correspond with geopotential height in dam at 60°S.

Intense cyclones selected solely on the basis of strong central vorticity (Figs. 7a–d) tend to be small and tight, with some variability in size as in Fig. 4. In comparison, the four storms possessing the strongest cyclonic circulation (Figs. 7e–h) are much larger systems having more open centers with weaker central vorticity. These appear to represent cyclones at a more mature stage of development than those in Figs. 7a–d and vary somewhat in the extent of strong gradient flow. The bottom row shows systems having both circulation *and* central vorticity above a threshold. The imposition of requirements on both vorticity and circulation seems to result in greater case to case homogeneity for these intense storms.

Of course, this limited sample is just a guide to possible case selection criteria. Other cyclone area or shape parameters are readily obtainable as by-products of the circulation calculations. Additional quantities derivable from the MSL pressure field such as geostrophic or gradient wind streamfunction, kinetic energy, or angular momentum can readily be computed for each track point and included as additional parameters in the cyclone database. Where multilevel gridded data are available, other parameters related to (say) orientation or strength of potential vorticity extrema, jet streaks, or frontal characteristics could also be included, depending on the goal of the study.

For cyclogenesis studies, various stages in a cyclone's life can be objectively identified from vorticity or circulation variations, as in SI95. Figure 8 shows the formation, development, maturity, and decay stages of the three storms in Figs. 7i–k. Here, formation was the first track point (or the beginning of circulation increases where a weak disturbance existed for several days before intensifying), development (decay) was the time when the cyclonic circulation was increasing (decreasing) most rapidly, while maturity was the stage of maximum circulation. Composites based on a large number of cyclones can then be constructed for each life cycle stage to determine persistent basic features, as in Manobianco (1989) and Sinclair and Cong (1992).

We have shown how an automated cyclone finding, tracking, and case selection rationale can greatly facilitate the selection of cyclones for case or composite studies from a long series of gridded analyses. However, it should be noted that objective case selection does not reduce the need for careful synoptic appraisal of each case selected.

5. Cyclone climatology

One means of assessing any objective procedure for tracking meteorological features is to compare results with the old, time-honored manual approach. In this section, a selection of winter season cyclone statistics for both hemispheres is obtained via the methodology outlined in this paper and compared with previous results. Only a brief survey of the climatological behavior of cyclones will be presented here. More detailed analysis, discussion, and interpretation of results will be saved for a future study.

For this survey, twice-daily ECMWF 1000-hPa geopotential analyses during 1980–94 (SH) and 1980–87 (NH) are used. These are first smoothed with a Cressman smoother ($r_o = 500$ km) and cyclones identified as maxima of cyclonic ζ_{gr} exceeding 1 CVU and tracked, as outlined earlier. Quasi-stationary orographic features are

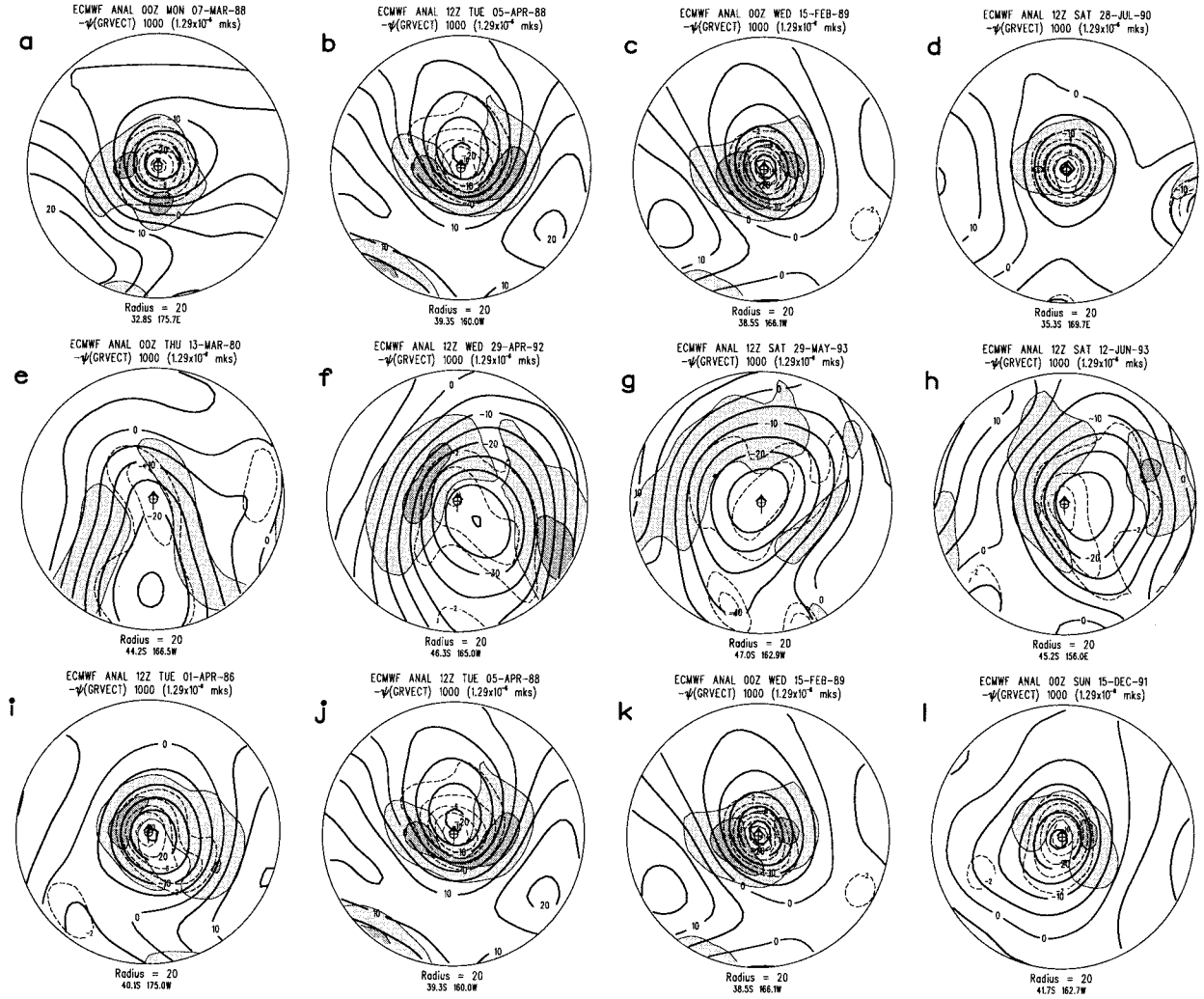

FIG. 7. Gradient wind streamfunction (solid, every 5 equivalent dam), cyclonic ζ_{gr} (dashed, every 2 CVU), and gradient wind >18 and 25 m s^{-1} (shaded) on a 20° latitude radius polar grid at the locations indicated below each plot for the indicated times, for 12 intense cyclones near New Zealand, selected from the database from the following criteria: (a)–(d) central $\zeta_{gr} > 12$ CVU, (e)–(h) circulation >14 CU, and (i)–(l) $\zeta_{gr} > 10$ CVU *and* circulation >10 CU.

removed and only cyclones lasting 2 or more days (four or more analyses) are considered.

a. Northern Hemisphere

Figure 9 shows a range of cyclone statistics for the NH winter (October–March). In Fig. 9a, a count of cyclone tracks passing within 5° latitude (555 km) of each grid point (''track density'') is obtained by counting centers just once per cyclone for each grid point. This measure of cyclone activity is similar to that used by Whittaker and Horn (1984) and indicates two principal regions of cyclone activity; one extending from near Japan toward the Gulf of Alaska and the other spiraling poleward from east of North America toward Iceland and the Arctic Ocean. Other localized maxima are seen over the Mediterranean Sea, the Great Lakes, east of the the Rockies, east of the Urals (near 80°E), and near the Caspian Sea. In all these details, Fig. 9a is quite similar to Fig. 2a of Whittaker and Horn (1984), based on manual analyses and tracking. Some differences exist over the middle latitudes of Asia, a region where MSL pressure fields are complicated by mountainous terrain and uncertain pressure reductions to sea level, and where data was missing during part of the analysis period in Whittaker and Horn's study.

Over the west-central Pacific, both Fig. 9a and Whittaker and Horn (1984) indicate maximum cyclone activity near 40°N. However, Gyakum et al. (1989), using a simple count of centers, found highest cyclone frequencies between 50° and 65°N, with localized maxima in the Gulf of Alaska and near Kamchatka Peninsula. Figure 10 shows that the differences between these studies are consistent with the differing methods used to

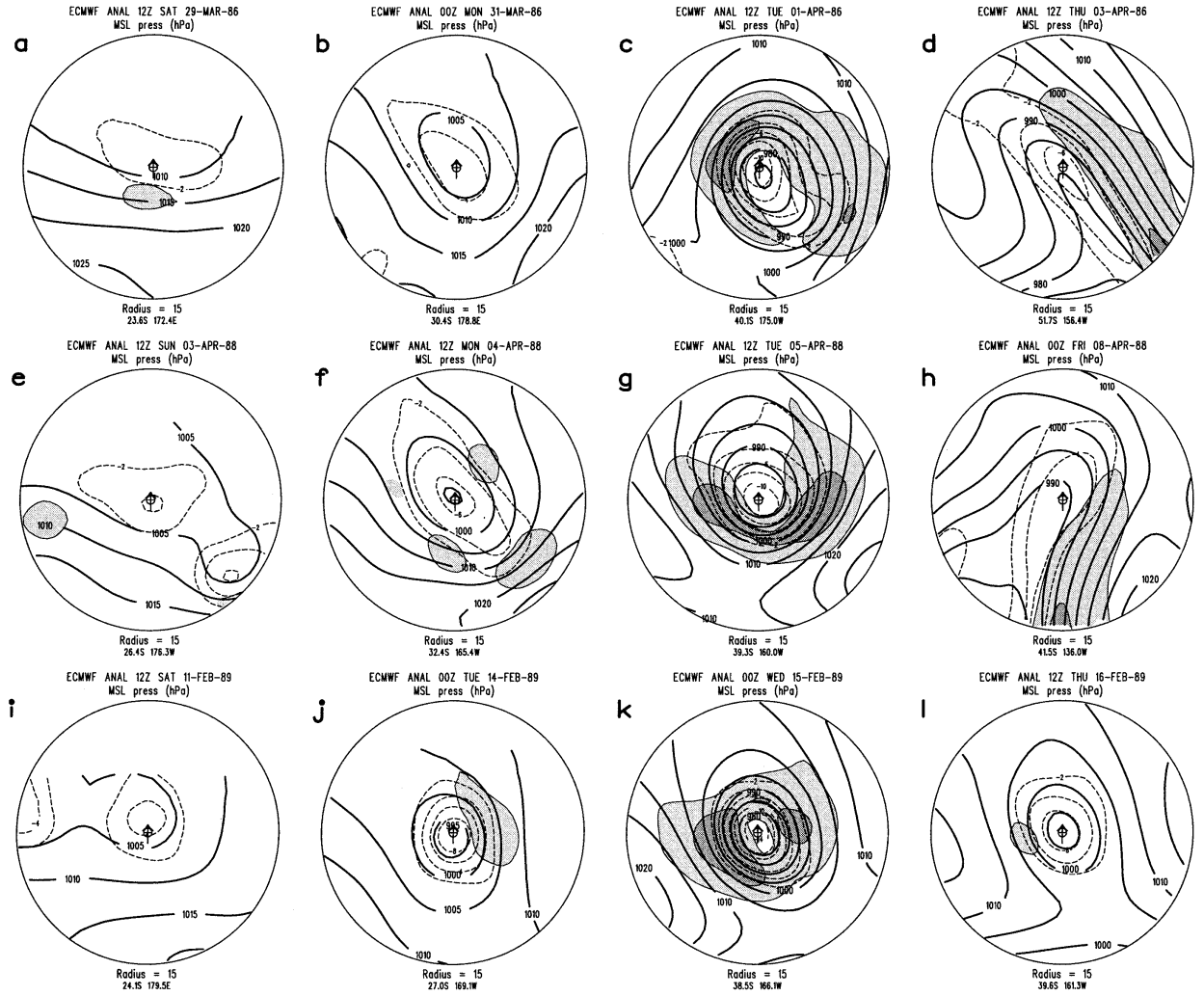

FIG. 8. MSL pressure (solid, every 5 hPa), cyclonic ζ_{gr} (dashed, every 2 CVU), and gradient wind >18 and 25 m s^{-1} (shaded) on a 15° latitude radius polar grid at the locations and time indicated near each plot for three cases of cyclogenesis. Four stages of development are shown: genesis (a),(e),(i), development (b),(f),(j), maturity (c),(g),(k), and decay (d),(h),(l). See text for more details.

count cyclones. In Fig. 10a, cyclones are counted using track density, as in Whittaker and Horn (1984) (and Fig. 9a), whereas a simple count of all centers without regard to tracking (''system density'') yields a distribution (Fig. 10b) close to that in Fig. 1 of Gyakum et al. (1989). Increased counts at higher latitudes in Fig. 10b and in Gyakum et al. (1989) arise because more than one count per track is allowed, giving extra weight to slower-moving systems in the Gulf of Alaska. Although changes in data coverage and intrinsic cyclone variability from year to year also contribute to differences between the earlier studies, these sources of variability appear smaller, as the year to year standard deviation (not shown) over the 7 yr considered here amounts to less than 20% of the contoured values in Fig. 9a, Other factors such as the present use of a Cressman smoother and the 1 CVU threshold for detecting a cyclone will also affect these comparisons. A more rigorous comparison involving application of an identical methodology to previous datasets is outside the scope of this study.

Average cyclone motion vectors are included in Fig. 9a. Cyclones are most mobile over the western Pacific near 35°N and between 40° and 50°N over North America and the western Atlantic. Cyclones have a mean poleward component of motion in the Gulf of Alaska and in the North Atlantic and an equatorward component east of the Rockies.

Instances of cyclone formation (Fig. 9b) are defined as all first track points having circulation weaker than 3 CU for cyclones ultimately attaining at least that intensity as tracked. As discussed in SI95, this definition excludes cyclones that remain weak during their life, as well as those that already have considerable circulation at the first track point. Favored genesis areas include the warm waters of the Kuroshio Current and Gulf Stream on the upstream equatorward flank of the mean

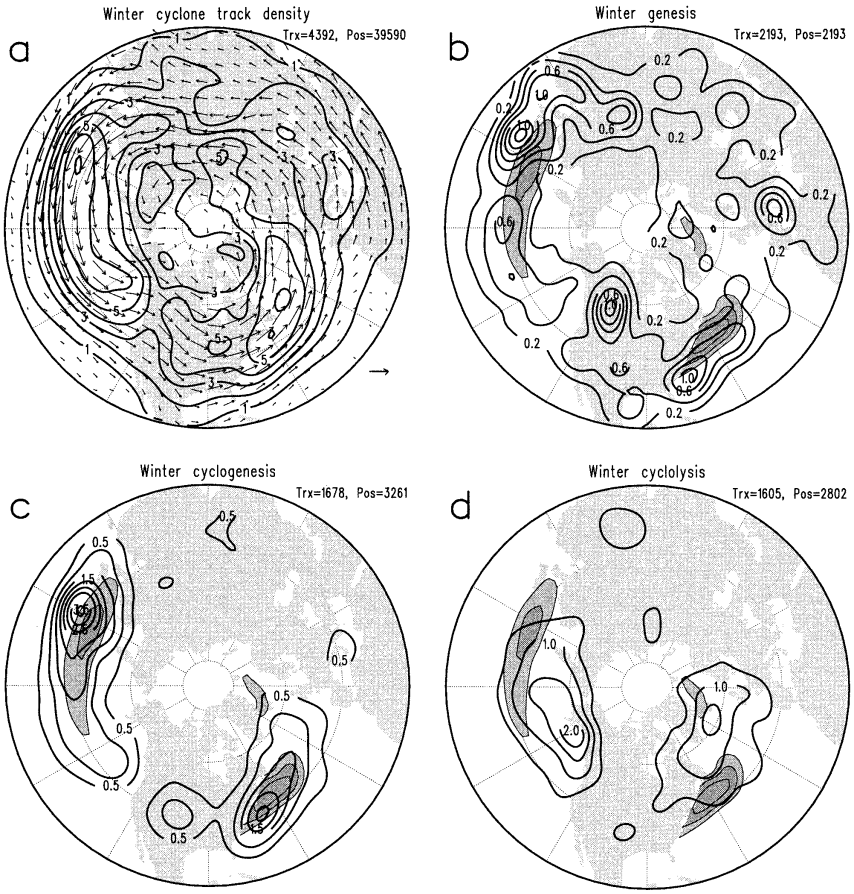

FIG. 9. Cyclone statistics for the Northern Hemisphere winter (October–March), for the years 1980–86. (a) Cyclone track density, drawn every 1 center (5° lat circle)$^{-1}$ month^{-1}, with average cyclone translation vectors added (the vector to the left represents 10 m s^{-1}). Count of (b) formation locations, every 0.2 (5° circle)$^{-1}$ month^{-1}, with SST gradient maxima exceeding 8° and 10°C (1000 km)$^{-1}$ added (shaded); (c) cyclogenesis locations, every 0.5 (5° circle)$^{-1}$ month^{-1}, with SST gradients as in (b); (d) cyclolysis locations, every 0.5 (5° circle)$^{-1}$ month^{-1}; (e) central vorticity changes >4 CVU, every 0.2 (5° circle)$^{-1}$ month^{-1}; (f) central pressure falls > 1 Bergeron, every 0.5 (5° circle)$^{-1}$ (month)$^{-1}$; and (g) tight (thick, solid) and open (thin solid) vortices, every 0.2 (5° circle)$^{-1}$ month^{-1}, with contour labels removed for clarity. The ''Trx'' and ''Pos'' values at the top right of each panel refer, respectively, to the numbers of cyclones (as tracked) and positions (centers) used for each plot.

SST gradient maxima (shaded) near the eastern seaboards of Asia and North America. Other formation regions are found near the date line, east of the Canadian Rockies and the Tibetan Plateau, over the western Mediterranean Sea, and near the Caspian Sea. These results are consistent with formation locations obtained manually by Whittaker and Horn (1984), Roebber (1984), and Gyakum et al. (1989), where they are discussed in more detail.

Winter cyclogenesis occurrences (Fig. 9c) were identified similarly to SI95 as instances where central vorticity increased faster than 2 CVU day^{-1}. Intensifying cyclones are found with highest frequency in two elongated zones extending downstream from the corresponding genesis regions over the eastern seaboards, adjacent to the maximum SST gradients in these regions. Colucci (1976), Whittaker and Horn (1984), and Roebber (1984) have also noted that the regions of strong SST gradients are conducive in a climatological sense to the development of maritime cyclones. Cycloysis (Fig. 9d) occurs well downstream from formation and development regions, and at higher latitudes (near 60°N), with maxima in the Gulf of Alaska and near Iceland.

The geographical distribution of rapid cyclogenesis events based on three different intensity change criteria are shown in Figs. 9e–g. Panel e shows the distribution of the 658 instances where the central vorticity increase following a storm exceeded 4 CVU day^{-1}. As for more moderate cyclogenesis events (Fig. 9c), rapidly intensifying cyclones are found in highest numbers on the equatorward flank of the maximum climatological SST gradient near the warm Kuroshio and Gulf Stream cur-

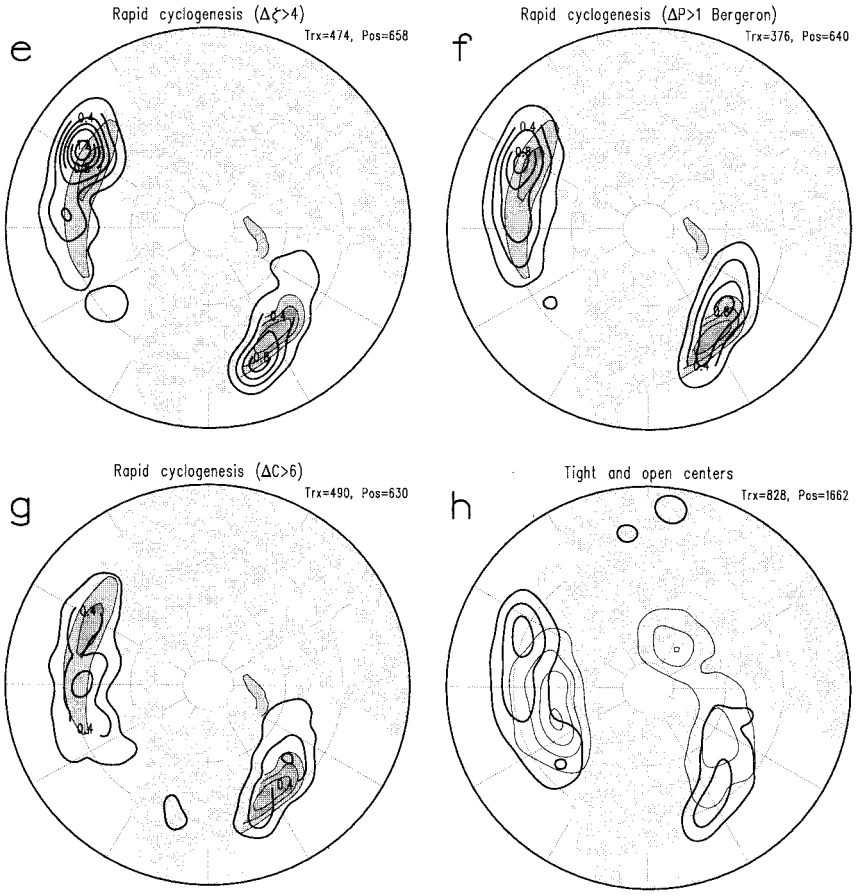

FIG. 9. (*Continued*)

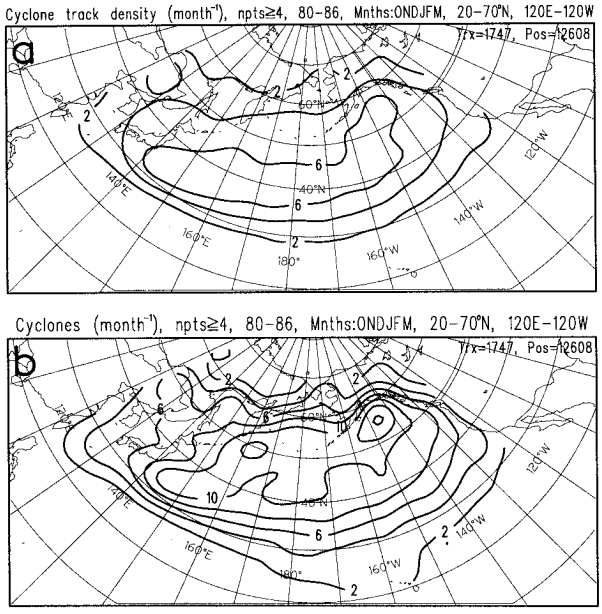

FIG. 10. Cyclone statistics for a portion of the North Pacific, for October–March for 1980–86. (a) Track density, every 2 (5°-lat radius circle)$^{-1}$ (month)$^{-1}$. (b) As in (a) except system density.

rents, with an additional smaller frequency maximum off the Pacific coast of Canada. The threshold vorticity change used for Fig. 9e was chosen to yield a similar sample size to cases having a pressure deepening rate >1 B. The geographical distribution of these rapid deepeners is shown in Fig. 9f. They occur slightly downstream from locations of strongest vorticity change (Fig. 9e) and have a distribution similar to that of ''bombs'' obtained by Roebber (1984) and Gyakum et al. (1989).

Instances of circulation increases >6 CU day^{-1} (Fig. 9g) occur even farther downstream from the region of vorticity increases and pressure falls, especially in the Pacific, suggesting that strengthening of the low-level cyclonic flow over a wider area occurs somewhat later in the cyclone's life. This has possible implications on mean cyclone structure. Figure 9h indicates that tighter vortices (those possessing large central vorticity to circulation ratios) as analyzed by the ECMWF are most frequent near eastern seaboards, while ''open'' systems possessing moderate or strong circulation but comparatively weak inner vorticity (like Figs. 4d and 7e–h) occur well downstream: in the Gulf of Alaska, southeast of Greenland, and in the Arctic Ocean. Of course, the present smoothed ECMWF analyses cannot resolve the

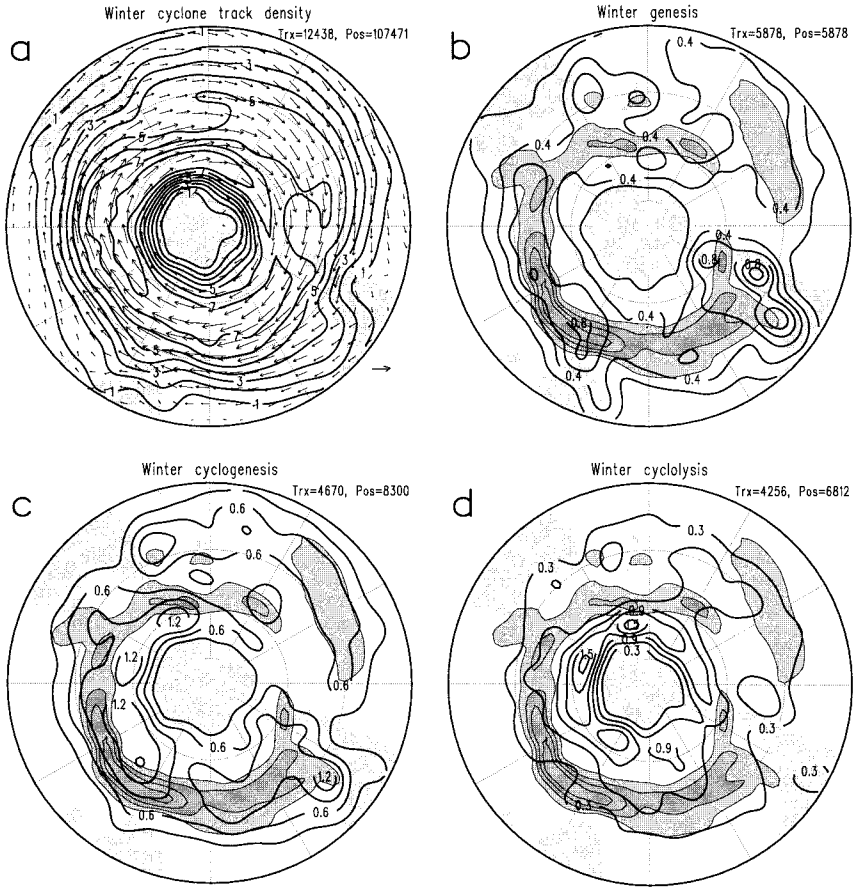

FIG. 11. As for Fig. 9 except for Southern Hemisphere winter (April–September) during 1980–94. SST gradients exceeding 6° and 8°C (1000 km)$^{-1}$ are shaded in panels (b)–(d). Contour intervals [number (5° lat radius circle)$^{-1}$ (month)$^{-1}$] are (a) 1, (b) 0.2, (c),(d) 0.3, (e) 0.05, (f),(g) 0.1, and (h) 0.2.

extreme inner core pressure gradients that occur in conjunction with ''coiled spring'' developments (Rogers and Bosart 1991). Another caveat is that the tightness of a particular center may be also linked to the availablility of observations near its center as well as to any intrinsic structure. Nevertheless, Fig. 9h is at least consistent with other circumstantial evidence (e.g., Reed et al. 1988) linking stronger inner pressure gradients with diabatic heating effects over the warm waters of the Gulf Stream and Kuroshio Current. In contrast, ''broader'' systems having comparatively weak inner vorticity appear to represent mature systems in a state of decay, occurring as they do in cyclolytic regions (cf. Fig. 9d) and over colder water.

In summary, NH cyclones tend to form over the warm waters of the Kuroshio Current and Gulf Stream and intensify near the region of strongest SST gradient as comparatively tight vortices. During their lives, they migrate eastward and poleward and expand in area before slowing and decaying in the Gulf of Alaska and near Iceland.

b. Southern Hemisphere

An identical set of statistics is presented for the SH (Fig. 11). Track density (Fig. 11a) maximizes between 50° and 60°S in the Atlantic and Indian Ocean sectors, and south of 60°S in the Pacific, with a broader secondary maximum spanning the Pacific near 40°S, consistent with similar results obtained by SI94 and SI95. Cyclones are most mobile around 50°S in the Indian Ocean sector. In comparison with the NH, the cyclone distribution of the SH exhibits a high degree of zonal symmetry. A count of centers without regard to tracking (not shown) highlights the slower-moving cyclones across New Zealand and the central Pacific, and those south of 60°S.

In comparison with SI94 and SI95, Fig. 11a depicts a shift toward higher latitudes. This is because SI94 and SI95 accumulated statistics on a polar stereographic domain without prior Cressman smoothing, favoring cyclone detection at lower latitudes where grid spacing is smaller (grid spacing at 30°S is 0.8 of that at 60°S).

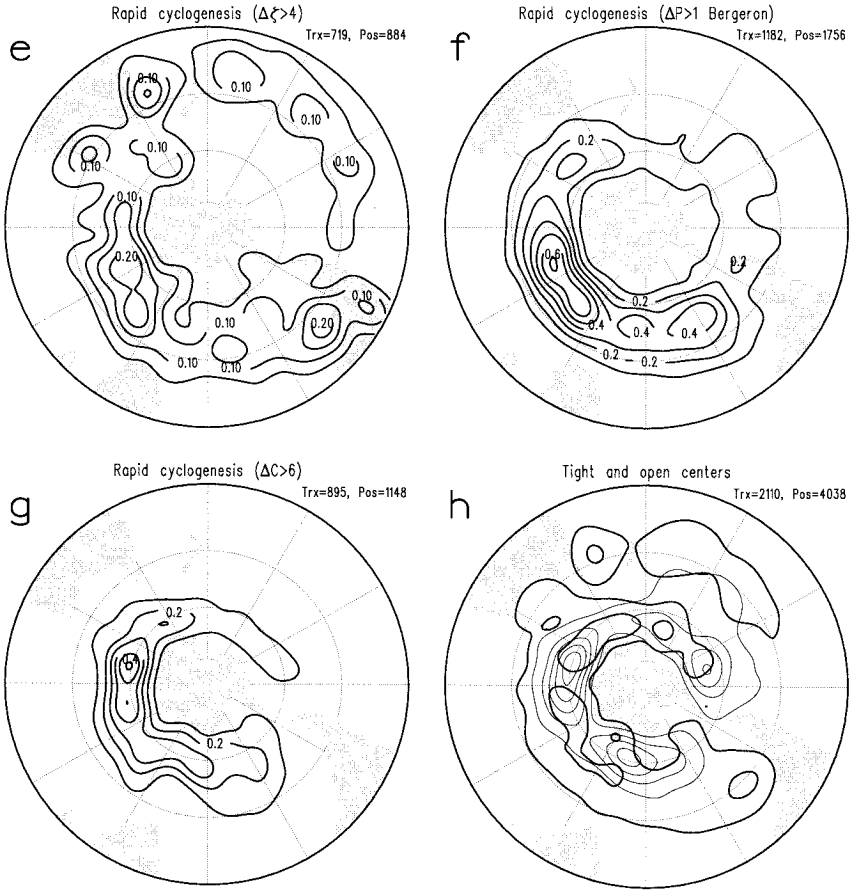

FIG. 11. (*Continued*)

However, this bias is smaller than the substantial high-latitude bias in previous studies based on detection of cyclones as pressure minima. As found by SI94, these studies exclude many mobile vorticity centers between 45° and 55°S while including large numbers of spurious orographic features near Antarctica. This again reinforces the need to ensure that the methods used to identify cyclones do not introduce bias.

Favored genesis locations (Fig. 11b) include eastern coasts of Australia and South America, across the Indian Ocean near the maximum SST gradient near 40°S, and in a broad region spanning the subtropical Pacific between 30° and 40°S, as in SI95. Cyclogenesis (Fig. 11c) is most prevalent downstream from these regions, maximizing east of South America, in a band extending from southeast of Africa into the high latitudes of the South Pacific, and throughout the middle latitudes of the Pacific sector. A relative minimum extends across the Pacific near 50°S. The double-occurrence maximum in the Pacific is thought to be related to the unique double-jet structure of the winter upper troposphere (SI95). Although the largest numbers of intensifying cyclones are found poleward of the strongest SST gradients in the Indian Ocean sector, the highest *fraction* (ratio of intensifying to all cyclones) is coincident with it (not shown). Dissipation locations (Fig. 11d) are overwhelmingly found poleward of 60°S, a region largely covered with sea ice in winter and spring.

Rapidly intensifying cyclones (Fig. 11e) are most frequent east of South America, southeast of Africa, in the Tasman Sea, and across the Pacific near 35°S, as in SI95. In contrast, rapid deepeners (Fig. 11f) are entirely confined to poleward of 40°S, with a preference for the Indian Ocean sector. As discussed by SI95, these differences between the distribution of developing cyclones as inferred from vorticity tendencies and those obtained from central pressure change are partly related to the unique climatological pressure field of the SH. Many instances of rapidly falling pressure are, in fact, artifacts of rapid poleward migration across the background mean pressure field (e.g., Figs. 3d–f).

Largest circulation increases (Fig. 11g) occur near 60°S. This is possibly due to the fact that cyclones in this region merge with the semipermanent climatological circumpolar trough, which involves considerable cyclonic circulation, even in its time-averaged state. Tighter vortices (Fig. 11h) tend to occur within the main cyclogenetic regions (cf. Fig. 11c), while more open

centers are found near 60°S. These results, of course, are subject to analysis uncertainty over these southern oceans.

This brief examination of SH cyclones, based on 15 years of data, extends the results of SI95 based on a shorter series of ECMWF analyses. The results in Fig. 11, based on the updated methodology, confirm the principal findings of SI94 and SI95, despite the low-latitude bias in those studies. The reader is referred to SI95 and the references therein for more detailed discussion and interpretation of the climatological behavior of SH cyclones.

6. Concluding remarks

This study has examined some of the issues associated with objectively identifying cyclones from numerical analyses. Modifications to the cyclone finding methodology of SI94 result in a cyclone database free from distortions arising from variations in grid spacing over the domain. This is accomplished by prior smoothing of the raw data using a constant radius Cressman-type spatial smoother to ensure that a known scale of disturbance is consistently admitted over the domain. This consistency is crucial where the goal is to look at small differences between cyclone behavior in different datasets (e.g., different GCMs).

Cyclones are identified as local maxima of cyclonic vorticity to eliminate a further bias favoring slower-moving or more intense cyclones that occurs when pressure minima are used. Orographic features not normally thought of as cyclones are also removed. A new procedure for estimating circulation is described. This assesses cyclone strength on the basis of both size and rotation rate, thus avoiding incongruities that occasionally arise with point measures such as central pressure or vorticity. Finally, an automated tracking scheme is used to generate a database of cyclone tracks containing center coordinates, pressure, vorticity, and circulation at each track point.

We have sketched an objective procedure for selecting cases from a cyclone track database obtained from an extended series of gridded MSL pressure charts. This avoids laborious manual examination of thousands of synoptic charts to find suitable storms. Case selection is instead done by computer search of the database for cyclones having specified properties. Selections can be on the basis of year, month, location, intensity (e.g., central pressure, vorticity or circulation), stage of development, and from intensity *change* characteristics.

Individual case studies based on intensive observational campaigns have revealed the rich palette of cyclone structures and life cycles found in nature. There is now a growing effort to bring much of this work together by attempting to classify cyclones on the basis of cloud signatures (e.g., Evans et al. 1994), precursor synoptic-scale flow patterns (e.g., Davies et al. 1991; Thorncroft et al. 1993), or adherence to various conceptual models (Bjerknes and Solberg 1922; Shapiro and Keyser 1990). Automated case selection from objectively derived track data incorporating such parameters at each track point as are germane to such classifications will increasingly be needed to assist with the huge task of assessing the relative importance of these paradigms for different regions of the globe.

Finally, we have applied the methodology to obtain a synoptic climatology for winter season cyclones in both hemispheres. Because the analyzed geographical distribution of cyclones is sensitive to the cyclone counting procedure, results in good agreement with previously published NH work based on the traditional manual approach are only found when care is taken to use a methodology consistent with the earlier studies. Discrepancies between earlier studies appear to primarily result from different counting methods, although intrinsic storm track variability and changes in analysis quality and data coverage undoubtedly also contribute. This finding reinforces a basic contention of this study: that care needs to be taken to ensure that a consistent methodology is used when comparing results from different datasets. The procedures outlined in this paper will help to ensure this consistency.

The present results, based on state-of-the-art operational numerical analyses that incorporate remotely sensed data not used in earlier manual studies, have confirmed the general picture of cyclone life cycles found in previous studies. Northern Hemisphere cyclones form and intensify near the eastern seaboards of Asia and North America, with activity focused on the regions of strongest SST gradient. They move eastward and poleward during their lives before weakening in the two principal NH cyclone graveyards: the Gulf of Alaska and southeast of Greenland. In comparison, SH cyclones are more evenly distributed around the hemisphere. They tend to form and intensify in middle latitudes, especially near SST gradients over open oceans, and near the eastern coasts of South America and Australia, and decay at higher latitudes. There is some evidence that newly formed and intensifying cyclones in both hemispheres possess a tighter inner structure than mature and decaying systems.

Thanks to the reanalysis efforts going on at NCEP and ECMWF, high quality multidecade datasets of numerically analyzed data are now becoming available. We hope to construct weather system tracks from these datasets to establish a benchline contemporary climatology that will advance our understanding of the behavior of these circulation systems and how they respond to and influence climate variability. Work is about to commence on obtaining cyclone statistics from a GCM to assess its ability in replicating contemporary weather system behavior and to identify possible shifts in storm characteristics under climate change scenarios. In this task, it will be essential

to ensure that small differences between different datasets are not artifacts of the cyclone finding methodology. Objective procedures such as described here will make all these tasks efficient and will ensure consistent, robust results.

Acknowledgments. Gridded atmospheric analyses were provided by the ECMWF, while the SST data in Figs. 9 and 11 were provided by the NCEP. Critical comments from three anonymous reviewers are appreciated, as they led to a substantially improved manuscript. This work was supported by the New Zealand Foundation for Research, Science and Technology.

APPENDIX

Calculation of Gradient Wind Vorticity

Because the gradient wind represents an improvement over the geostrophic as an approximation to the real wind, we estimate the gradient wind field and determine its vorticity. This estimate is based on the gradient wind equation

$$KV^2 + fV = fV_g, \tag{A1}$$

where $V(V_g)$ is the gradient (geostrophic) wind, f is the Coriolis parameter, and K the curvature of the parcel trajectory. Here, we have approximated K by the isobar curvature, computed (after Trenberth 1977) as

$$\frac{\partial^2\Phi/\partial x^2(\partial\Phi/\partial y)^2 - 2(\partial\Phi/\partial x)(\partial\Phi/\partial y)\partial^2\Phi/\partial x\partial y + \partial^2\Phi/\partial y^2(\partial\Phi/\partial x)^2}{[(\partial\Phi/\partial x)^2 + (\partial\Phi/\partial y)^2]^{3/2}}, \tag{A2}$$

where Φ is the geopotential, $\partial/\partial x$ is approximated as $(1/a\cos\phi)\partial/\partial\lambda$, and $\partial/\partial y$ is $\partial/a\,\partial\phi$ (ϕ, λ are latitude, longitude in radians, and a is the mean earth radius). Cyclonic curvature is positive (negative) in the NH (SH) and has units per meter. The solution technique for (A1) uses an iterative technique, where V_g is used as a first guess, V_1 to V in a rearranged version of (A1),

$$V_n = V_g/(1 + KV_{n-1}/f). \tag{A3}$$

Here, the quantity KV_{n-1}/f in (A3) is constrained to lie between -0.25 and 0.5, limiting the gradient wind speed to between $2V_g/3$ and $4V_g/3$, with smaller (larger) values for cyclonic (anticyclonic) flow. These limits were empirically found to yield closest agreement with observed wind in another dataset containing U and V in addition to H (see below). For the spatially smoothed data used here, these limits were only occasionally reached in the subtropics. For normal-gradient wind balance, the theoretical range is between zero and $2V_g$, with the upper limit required for real solutions to (A1). The vorticity of the gradient wind, ζ_{gr}, was then calculated as

$$\zeta_{gr} = \partial v/\partial x - \partial u/\partial y + u\tan\phi/a, \tag{A4}$$

where u and v are the eastward and northward components of the gradient wind. Centered differences were used to compute the derivatives, with calculations limited to poleward of 20° latitude.

This algorithm was evaluated by comparing ζ_{gr}, as obtained above, with vorticity, ζ, obtained directly from contemporaneous U and V analyses. Comparisons were based on a set of 258 gridded 1000-hPa ECMWF analyses during 1990. These contained U and V in addition to H on the 2.5° × 2.5° grid over a region bounded by 20°–60°S and 130°E–130°W. Gradient wind vorticity was computed as outlined above from H and compared (over each grid point of each analysis) with ζ obtained directly from U and V. A similar comparison was made for geostrophic vorticity, ζ_g. Cressman smoothing was as specified in section 2. Despite the approximations inherent in the calculation of gradient winds, average ζ_{gr} estimates were closer to ζ than ζ_g values, with an overall rms difference between ζ_{gr} and ζ of 0.68 CVU compared to 0.79 for ζ_g. When the comparison was made for just cyclonic values, the rms difference for ζ_g was more than 1 CVU compared with just 0.76 CVU for ζ_{gr}. In regions where cyclonic vorticity >5 CVU (cf. Figs. 1 and 8), ζ_g systematically overestimated ζ by nearly 3 CVU compared with just 1 CVU for ζ_{gr}, with rms differences of 3.2 and 1.3, respectively. Thus, the gradient wind approximation as used here appears to yield improved vorticity estimates over geostrophic values, especially in the environs of cyclones, as applied in this study.

REFERENCES

Akyildiz, V., 1985: Systematic errors in the behaviour of cyclones in the ECMWF operational models. *Tellus,* **37A,** 297–308.

Bell, G. D., and L. F. Bosart, 1989: A 15-year climatology of Northern Hemisphere 500-mb closed cyclone and anticyclone centers. *Mon. Wea. Rev.,* **117,** 2142–2163.

Bjerknes, J., and H. Solberg, 1922: Life cycle of cyclones and the polar front theory of atmospheric circulation. *Geofys. Publ.,* **3** (1), 1–18.

Bleck, R., 1965: Linear approximations for determining one and two-dimensional numerical filters in dynamical meteorology (in German). [Available from Institute for Theoretical Meteorology, Free University of Berlin, Berlin, Germany.]

Bullock, T. A., and J. R. Gyakum, 1993: A diagnostic study of cyclogenesis in the western North Pacific. *Mon. Wea. Rev.,* **121,** 65–75.

Carleton, A. M., 1979: A synoptic climatology of satellite-observed

extratropical cyclone activity for the Southern Hemisphere winter. *Arch. Meteor. Geophys. Bioklimatol. B,* **27,** 265–279.

Colucci, S. J., 1976: Winter cyclone frequencies over the eastern United States and adjacent western Atlantic 1964–73. *Bull. Amer. Meteor. Soc.,* **57,** 548–553.

Cressman, G. P., 1959: An operational objective analysis system. *Mon. Wea. Rev.,* **87,** 367–374.

Davies, H. C., C. Schär, and H. Wernli, 1991: The palette of fronts and cyclones within a baroclinic wave development. *J. Atmos. Sci.,* **48,** 1666–1688.

Evans, M. S., D. Keyser, L. F. Bosart, and G. M. Lackmann, 1994: A satellite-derived classification scheme for rapid maritime cyclogenesis. *Mon. Wea. Rev.,* **122,** 1381–1416.

Gyakum, J. R., Anderson, R. H. Grumm, and E. L. Gruner, 1989: North Pacific cold season surface cyclone activity: 1975–1983. *Mon. Wea. Rev.,* **117,** 1141–1155.

——, P. J. Roebber, and T. A. Bullock, 1992: The role of antecedent surface vorticity development as a conditioning process in explosive cyclone intensification. *Mon. Wea. Rev.,* **120,** 1465–1489.

Jones, D. A., and I. Simmonds, 1993: A climatology of Southern Hemisphere extratropical cyclones. *Climate Dyn.,* **9,** 131–145.

——, and ——, 1994: A climatology of Southern Hemisphere anticyclones. *Climate Dyn.,* **10,** 333–348.

Kidson, J. W., and M. R. Sinclair, 1995: The influence of persistent anomalies on Southern Hemisphere storm tracks. *J. Climate,* **8,** 1938–1950.

König, W., R. Sausen, and F. Sielmann, 1993: Objective identification of cyclones in GCM simulations. *J. Climate,* **6,** 2217–2231.

Lambert, S. J., 1988: A cyclone climatology of the Canadian Climate Centre General Circulation Model. *J. Climate,* **1,** 109–115.

Lefevre, R. J., and J. W. Nielsen-Gammon, 1995: An objective climatology of mobile troughs in the Northern Hemisphere. *Tellus,* **47A,** 638–655.

Le Marshall, J. F., and G. A. M. Kelly, 1981: A January and July climatology of the Southern Hemisphere based on daily numerical analyses 1973–77. *Aust. Meteor. Mag.,* **29,** 115–123.

Le Treut, H., and E. Kalnay: 1990: Comparison of observed and simulated cyclone frequency distribution as determined by an objective method. *Atmosfera,* **3,** 57–71.

Manobianco, J., 1989: Explosive East Coast cyclogenesis over the west-central North Atlantic Ocean: A composite study derived from ECMWF operational analyses. *Mon. Wea. Rev.,* **117,** 2365–2383.

Murray, R. J., and I. Simmonds, 1991a: A numerical scheme for tracking cyclone centres from digital data. Part I: Development and operation of the scheme. *Aust. Meteor. Mag.,* **39,** 155–166.

——, and ——, 1991b: A numerical scheme for tracking cyclone centres from digital data. Part II: Application to January and July general circulation model simulations. *Aust. Meteor. Mag.,* **39,** 167–180.

——, and ——, 1995: Responses of climate and cyclones to reductions in Arctic Winter sea ice. *J. Geophys. Res.,* **100C,** 4791–4806.

Reed, R. J., A. J. Simmons, M. D. Albright, and P. Unden, 1988: The role of latent heat release in explosive cyclogenesis: Three examples based on ECMWF operational forecasts. *Wea. Forecasting,* **3,** 217–229.

Roebber, P. J., 1984: Statistical analysis and updated climatology of explosive cyclones. *Mon. Wea. Rev.,* **112,** 1577–1589.

Rogers, E., and L. F. Bosart, 1991: A diagnostic study of two intense oceanic cyclones. *Mon. Wea. Rev.,* **119,** 965–996.

Sanders, F., 1986: Explosive cyclogenesis in the west-central North Atlantic Ocean, 1981–84. Part I: Composite structure and mean behavior. *Mon. Wea. Rev.,* **114,** 1781–1794.

——, and J. R. Gyakum, 1980: Synoptic-dynamic climatology of the ''bomb.'' *Mon. Wea. Rev.,* **108,** 1589–1606.

Shapiro, M. A., and D. Keyser, 1990: Fronts, jet streams, and the tropopause. *Extratropical Cyclones, The Erik Palmén Memorial Volume,* C. W. Newton and E. O. Holopainen, Eds., Amer. Meteor. Soc., 167–191.

Simmonds, I., and X. Wu, 1993: Cyclone behaviour response to changes in winter Southern Hemisphere sea ice concentration. *Quart. J. Roy. Meteor. Soc.,* **119,** 1121–1148.

Sinclair, M. R., 1994: An objective cyclone climatology for the Southern Hemisphere. *Mon. Wea. Rev.,* **122,** 2239–2256.

——, 1995: A climatology of cyclogenesis for the Southern Hemisphere. *Mon. Wea. Rev.,* **123,** 1601–1619.

——, 1996: A climatology of anticyclones and blocking for the Southern Hemisphere. *Mon. Wea. Rev.,* **124,** 245–263.

——, and X. Cong, 1992: Polar air stream cyclogenesis in the Australasian region: A composite study using ECMWF analyses. *Mon. Wea. Rev.,* **120,** 1950–1972.

Streten, N. A., and A. J. Troup, 1973: A synoptic climatology of satellite observed cloud vortices over the Southern Hemisphere. *Quart. J. Roy. Meteor. Soc.,* **99,** 56–72.

Taljaard, J. J., 1967: Development, distribution and movement of cyclones and anticyclones in the Southern Hemisphere during the IGY. *J. Appl. Meteor.,* **6,** 973–987.

Thorncroft, C. D., B. J. Hoskins, and M. E. McIntyre, 1993: Two paradigms of baroclinic wave life-cycle behavior. *Quart. J. Roy. Meteor. Soc.,* **119,** 17–55.

Trenberth, K. E., 1977: Objective numerical analysis of geopotential height fields in New Zealand. New Zealand Meteorological Service Tech. Information Circular 158, 21 pp. [Available from MetService, P.O. Box 722, Wellington, New Zealand.]

——, 1991: Storm tracks in the Southern Hemisphere. *J. Atmos. Sci.,* **48,** 2159–2178.

——, 1992: Global analyses from ECMWF and atlas of 1000 to 10 mb circulation statistics. NCAR Tech. Note NCAR/TN-373+STR, 191 pp. [Available from NCAR, P.O. Box 3000, Boulder, CO 80307.]

Whittaker, L. M., and L. H. Horn, 1984: Northern Hemisphere extratropical cyclone activity for four mid-season months. *J. Climatol.,* **4,** 297–310.